Rolling Prevention Mechanism for Underground Pipe Erosion Inspection Robot with a Real Time Vision System

Liqiong Tang, Massey University, Palmerston North, New Zealand

Donald Bailey, Massey University, Palmerston North, New Zealand

Matthieu Jones, Massey University, Palmerston North, New Zealand

ABSTRACT

Pipe inspection is one of the areas that have attracted high research interest for robot applications especially in oil and chemical industry and civil engineering. Robot body rolling while it travels within a pipe has been a problem for accurately collecting inspection data. Under certain circumstances where vision systems have to be employed, robot body rolling may cause vision inspection data to have little value as it is difficult to know where exactly the camera was looking at. This paper proposes an anti-rolling mechanism to hold consistent camera orientation. By changing the position angle of the robot legs, the mechanism is able to adjust the resistance to rolling within a pipe, therefore preventing robot rolling happening. The design makes use of the friction force caused by the gravity force of the robot to prevent the robot body rolling. The design analysis quantifies the effect of pipe radius, robot weight, payload, and payload offset distance in robot rolling. A test model was built based on the design concept. The experimental results obtained from the test model match the predication of the computational analysis. A real time vision system has been developed using FPGA and the algorithm of the structured laser light stripe configuration in the context of pipe inspection. The real-time hardware implementation of the algorithms on the robot itself removes the need to transmit raw video data back to an operator.

Keywords: *Anti-Rolling Mechanism, Field-Programmable Gate Array (FPGA), Image Processing, Pipe Inspection, Robot Body Rolling, Robot Design*

Concrete wastewater pipes are commonly used in chemical and process industries. As concrete is susceptible to acid erosion, when the PH of the wastewater is below 6.5, erosions occur on the wall of the wastewater pipes and gradually lead to the contents of the pipe leaking to the surroundings. Erosion of wastewater pipes is a huge problem for many chemical and process industries. As wastewater pipes are often underground and hard to access, repairing or replacing the eroded pipes is both timely and costly especially if the actual need for repair-

DOI: 10.4018/ijimr.2013070105

ing is unknown. A robotic system that is able to inspect the erosion inside of the pipes can provide a clear understanding of the situation, determine the location of the eroded areas, and make an accurate assessment of the damage before taking any corrective action.

Repairing or replacing concrete wastewater pipes requires extensive excavation of the pipes. However, any assumption that the pipes always have a bottom for the robot to run on is not appropriate for this case. As most of the time wastewater pipes are not run full, only the bottom surface of the pipes is most frequently in contact with wastewater and the damage often occurs only on the bottom of the pipes. In severe cases, the bottom surface of the pipes can be completely eroded away as shown in Figure 1. This sets a challenge for a robot with a vision system to accurately locate the eroded areas and determine the extent of erosion. The capability to travel inside a wastewater pipe with no bottom surface and provide a steady platform for real time vision system become the essential requirements for a pipe inspection robot.

This paper presents a proof of concept design for a pipe robotic system that has a potential to be used for concrete wastewater pipe inspection. The data captured must provide a profile of the erosion to map the position and the extent of the eroded areas. This requires the robot platform stably holding its orientation while it travels through the pipe to prevent the vision system rendering any results irrelevant. The research has been focused on wastewater pipes that are straight sections of horizontal pipes and joined at regular intervals from 15 to 50 meters with a manhole. The diameters of the pipes range from 250 to 400mm. The required accuracy of the erosion profile is set to be one millimeter for the depth measurement and one to two millimeters and 5-20 millimeters for the position of the erosion across the pipe and along the pipe centre line respectively.

ROLLING PREVENTION MECHANISM

Conceptual Design

Research study shows a rich content of pipe robot design for different applications (Roman et al., 1993; Yaguchi & Izumikawa, 2012; Roh et al., 2001; Pfeiffer et al., 2000; Ryew et al., 2000), but few are really applicable for this research. To meet the specific requirements, the conceptual design of the robot's mechanical system has a rectangular platform supported by four wheeled legs as illustrated in Figure 2. The four robot legs are identical and interchangeable, as are the wheels. The legs are assembled with the robot platform through two rotational joints located at the centre of the two ends of the platform.

Figure 1. Pipe erosion concentrated at the bottom of the pipe

Suppose the origin of a Cartesian coordinate system is set coincidently at the centre point of the robot platform, with the Z-axis collinear with the pipe centre line, X-axis horizontal and Y-axis vertical, as illustrated in Figure 2. If the robot platform is placed horizontally inside the pipe with the center point of the line that joins the two rotational joints coincidently located at the origin of the Cartesian coordinate system, then the center line of the rotational joints for the robot legs is collinear with the pipe centre line as shown in Figure 2, where W the robot gravity force, R the pipe radius, F_a and F_b are the normal forces applied on the robot wheels. To simplify the analysis, the gravity forces of the robot legs are ignored; also assume the design of the robot is symmetric with respect to both the XOY and YOZ planes.

Angle θ is the angle measured in front view from the top surface of the robot platform to the robot leg. The assembly allows the robot legs to rotate around the centre of the rotational joint. This makes angle θ adjustable. When the robot platform is placed horizontally, as the design is symmetric, the assembled mechanism guarantees the centre of the gravity is always below the top surface of the platform. Under ideal conditions, the gravity centre of the robot should be on the Y-axis and in the longitudinal vertical plane that passes through the pipe centre line.

Force Analysis Without Payload

In the static state, with no payload on the robot platform, the symmetric design with respect to the XOY and YOZ planes assures the forces applied on the robot satisfy the equilibrium condition.

$$(F_a - F_b) * Cos\theta = 0 \quad (1)$$

$$(F_a + F_b) * Sin\theta - W = 0 \quad (2)$$

Figure 2. The front view of the conceptual design of the pipe inspection robot

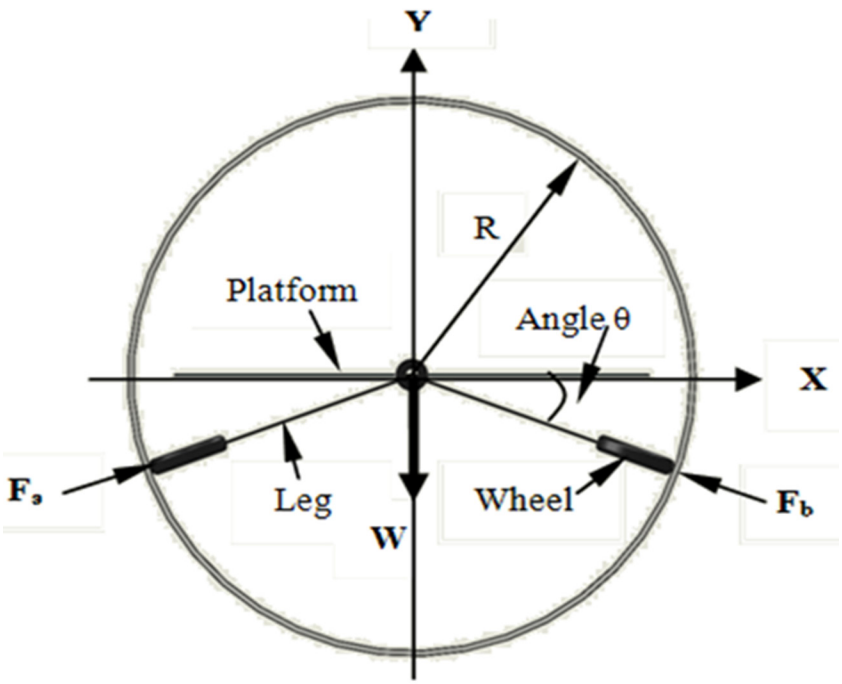

where F_a and F_b are the sum of the normal forces applied to the left and right sides of the robot wheels.

As a result:

$$F_a = F_b = \frac{W}{2 * Sin\theta} \quad (3)$$

Equation 3 indicates F_a and F_b changes with angle θ. The rational domain for angle θ is $0 < \theta \leq 90$. For a unit mass, the θ - F_a graph is shown in Figure 3. The graph reveals that, when θ is less than 20 degrees and approaches to 0 degree, the value of F_a increases rapidly and approaches to infinity. Apparently an applicable boundary for angle θ must be considered. Based on the θ - F_a graph, the lower limit for angle θ set at 20 degrees is a reasonable approach for the study of the normal forces applied on the robot wheels.

Friction Forces on Robot Wheels

Re-examining the forces applied on the robot shown in Figure 2, W, F_a and F_b do not directly generate any rolling torques. The contributors to robot rolling are the friction forces applied on the robot wheels. The friction forces between the robot wheels and the pipe internal surface depend on the normal forces applied on the robot wheels and the frictional coefficient μ. The frictional coefficient depends on the working condition and the materials of the pipe and the robot wheels. Once the working environment is fixed and the materials are chosen, the possible factor that changes the friction force is the normal force applied on the robot wheel. For the case of this study, as shown in Figure 3, angle θ has significant influence on the magnitude of the normal force. For a constant frictional coefficient μ, there is a possibility to generate enough friction forces on the robot wheels to prevent robot rolling through the adjustment of angle θ.

Figure 3. The θ - F_a graph

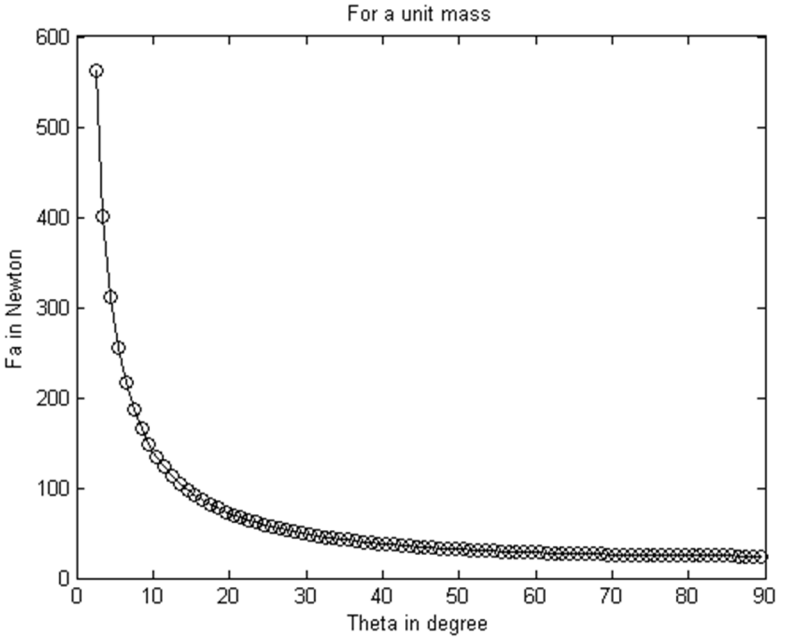

For this research, the wastewater pipe is made of concrete. The working condition inside of a wastewater pipe is damp and can be slippery. Referring to the frictional coefficient for static and sliding friction recommended by Roymech.co.uk and Engineeringtoolbox.com, the close recommended values for the frictional coefficient μ is from 0.1 to 0.85, which is based on the consideration of the sliding and static friction between smooth tires and wet concrete surface.

Force Analysis with an Offset Payload

Consider a load W_{load} placed on the robot platform with an offset distance D, as illustrated in Figure 4, where f_a and f_b are the friction forces applied on the robot wheels. For the robot to be in the equilibrium state, the external forces and torques acting on the robot have to be balanced (Norton, 2011; Budynas & Nisbett, 2008).

$$(F_a - F_b) * Cos\theta + \mu * (F_a + F_b) * Sin\theta = 0 \tag{4}$$

$$(F_a + F_b) * Sin\theta - \mu * (F_a - F_b) * Cos\theta - W - W_{load} = 0 \tag{5}$$

$$D * W_{load} - (f_a + f_b) * R = 0 \tag{6}$$

Therefore:

$$F_a = \frac{F_b(\cos\theta - \mu\sin\theta)}{\cos\theta + \mu\sin\theta} \tag{7}$$

$$F_b = \frac{(W + W_{load})(\cos\theta + \mu\sin\theta)}{2\sin\theta\cos\theta(1+\mu^2)} \tag{8}$$

$$D = \frac{\mu R(W + W_{load})}{W_{load} * \sin\theta * (1+\mu^2)} \tag{9}$$

Equation 9 presents the elements that affect the allowed offset distance D without robot rolling. This means if a load such as the

Figure 4. Robot with an offset load

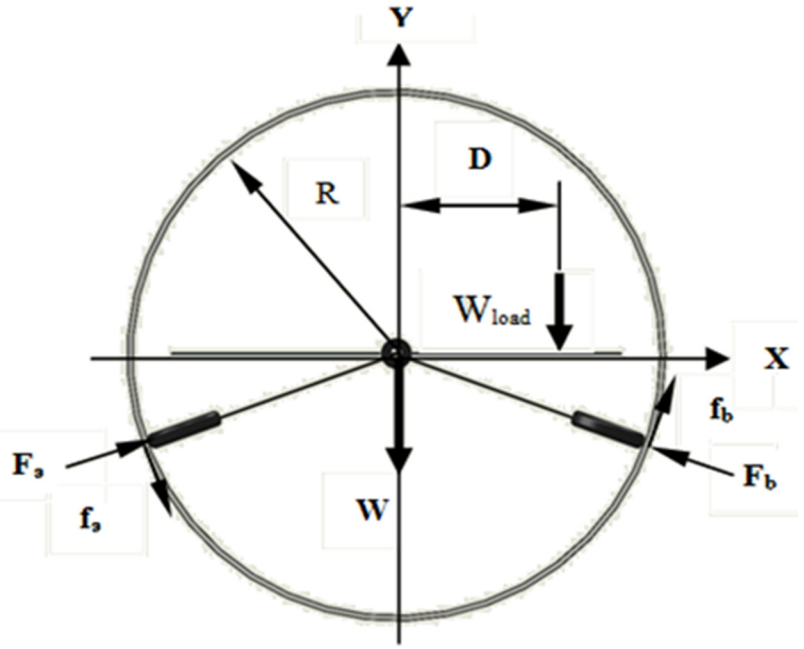

motor drivers, control board and vision system is placed on the robot platform away from the centre line of the platform, as long as the load is within the distance D, it will not cause the robot body to roll. For a given robot with a known payload and a pipe with a fixed radius, the only two remaining elements that affect the offset distance D are the friction coefficient μ and angle θ. MATLAB was used to study the case and further understand the influence of μ and θ, and calculate the limits of the offset distance D before robot rolling happens.

Suppose the pipe radius R, the robot weight W and the offset load W_{load} make a unit offset distance, then the offset distance D defined by Equation 9 can be written as a function of θ and μ.

$$D = f(x) = f\left(\frac{\mu}{\sin\theta * (1+\mu^2)}\right) \tag{10}$$

where $\theta \neq 0$

Figure 5 shows the corresponding D-θ-μ graph. The graph indicates that, as angle θ decreases and the coefficient μ increases, the offset distance D increases, which means the possibility to have the robot rolling is reduced. In reality, when the robot starts to travel, the value of μ is smaller especially for wheel based pipe robot. In a practical application, the value of μ depends on the materials of the pipe, the robot, the pipe condition such as dry or wet, etc. Equation 10 and Figure 5 can be used as a reference for placing the load on the robot platform without causing robot body rolling.

We follow the same philosophy to obtain the D-R-μ graph. Considering the recommended value for angle θ in and earlier section (20 degrees) and assuming the robot weight, offset load and angle θ make a unit offset distance, then the offset distance D is a function of pipe radius R and the friction coefficient μ. Figure 6 is the corresponding D-R-μ plot. It clearly shows the offset distance is positively proportional to the pipe radius.

For this research, the chosen wastewater pipe has a radius of 155mm. The robot weighs 5kg and is able to carry a load of up to 2kg. In ad-

Figure 5. The plot describing the effects of θ and μ on D

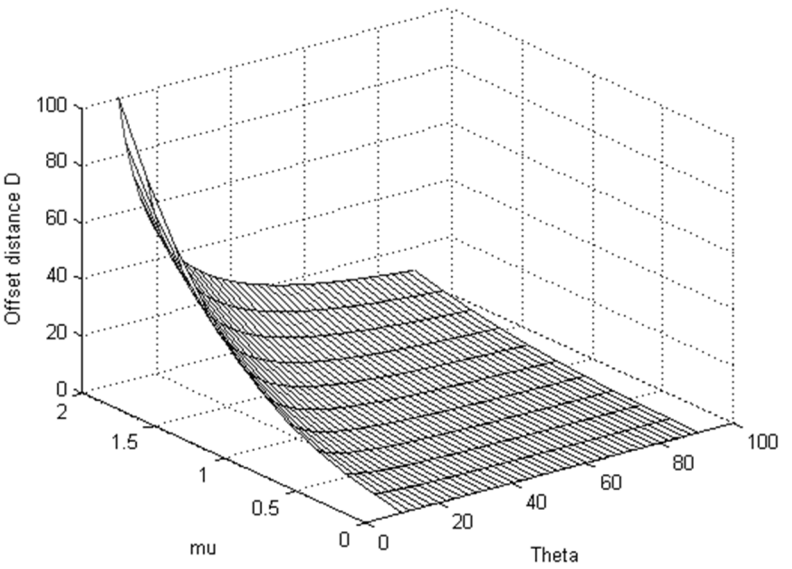

dition to these requirements, the recommended values for angle θ and the friction coefficient μ are used for the study. MATLAB was employed to analyze the possible behavior of the robot and calculate the offset distance before robot rolling happens.

The study first investigated the influence of angle θ and friction coefficient μ on the offset distance D based on the recommended values for both θ and μ. Figure 7 is the outcome of the analysis under the assumption of the robot weight is 5kg. The plot in Figure 7 shows that, when angle θ is 20 degrees, even μ takes the lowest value 0.1, which generates the smallest friction force on the robot wheel, the allowed offset distance D for the load can still reach 155mm without causing robot rolling. This offset distance reaches the radius of the given pipe. It means a 2kg offset load can be freely placed on either side of the robot platform without causing robot rolling within the wastewater pipe. This is because the normal forces caused on the wheels by the 5kg robot generated enough friction force to prevent the robot rolling. The analysis also reveals that, for a given offset load and a fixed pipe radius, the higher value of μ and the larger value of the angle θ should be considered to reduce normal force applied on the robot wheels, and as a result, reducing the power consumption.

The study in an earlier section shows that the preferred value for angle θ is not less than 20 degrees. The following investigation focused on the influence of the offset load W_{load} and the friction coefficient μ for a fixed angle θ. The D-W_{load}-μ graph in Figure 8 is obtained under the condition where angle θ is 20 degrees, W_{load} varies from 0.5 to 4 kg, and μ changes from 0.1 to 0.4. For the case where the offset load is less than 2kg, pipe radius equals to 155mm and the robot weighs 5kg, as long as the coefficient μ is less than 0.1, no matter where the offset load is placed on the robot platform, it will not cause robot rolling. The D-W_{load}-μ plot can be used as the basis to estimate the offset

Figure 6. The plot describing the effects of R and μ on D

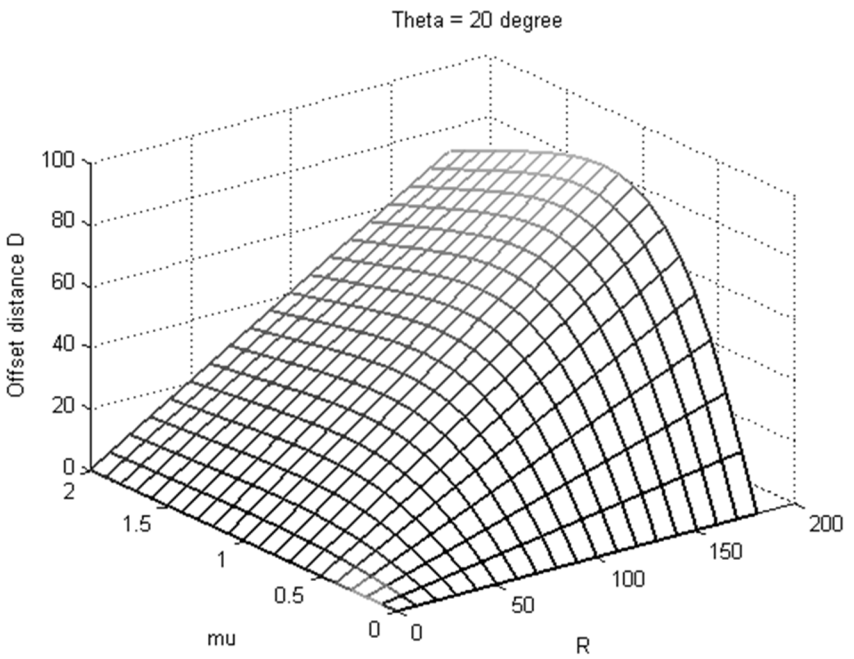

Figure 7. The D-θ-μ plot for a given R, W and W_{load}

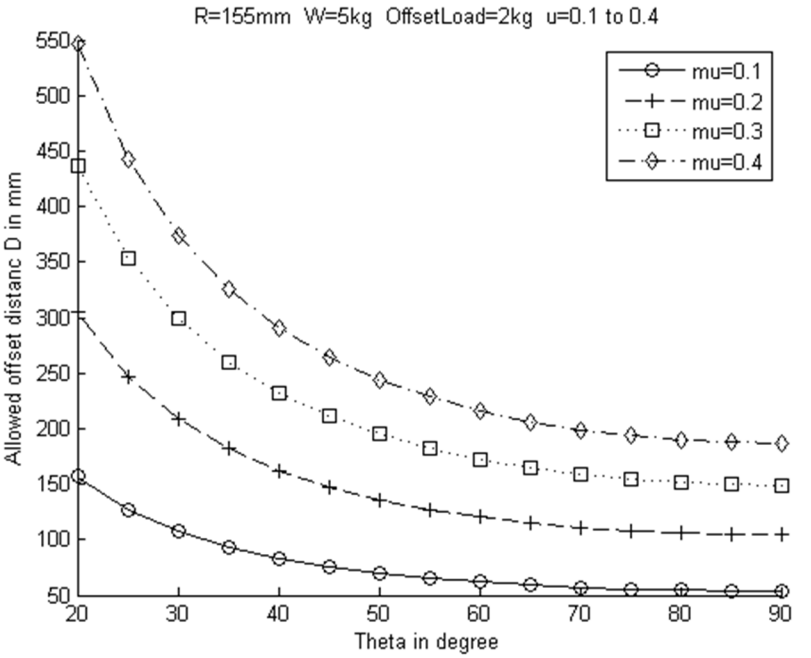

distance for different offset load, with angle θ fixed at 20 degrees.

Further investigation focused on the relation between the offset distance D and pipe radius R with a fixed robot weight W, offset load W_{load} and angle θ. Figure 9 shows the influence of R and μ on D for a condition where W=5kg, W_{load} =2kg and θ =20 degrees. The D-R-μ graph indicates that, for a given offset load and angle θ, as the pipe radius R increases, the allowed offset distance D increases. For a pipe with a radius of 155mm, even μ with the smallest value 0.1, the robot is still able to hold the orientation of the robot platform even with the offset load placed over 100mm away from the pipe centre line.

PROTOTYPE DEVELOPMENT AND TESTING

The investigation in the previous sections presented the influence and contribution from the possible variables such as the robot weight, pipe radius, and friction coefficient on the offset distance D. However, the previous analysis was a static analysis. In reality, the robot performance will be different when the robot moving down the pipe as the wheels will never be perfectly aligned. A torque will definitely exist and try to make the robot corkscrew down the pipe. The safe way is to place any load on the robot platform at much smaller distance than the allowed offset distance D. Also the adjustment of angle θ to change the friction forces on the wheels is another way to improve the behavior of the robot and prevent it from rolling.

Considering the requirements set by this industrial task, and based on the outcome of the previous analysis, a physical test model was built to confirm the concept design of the pipe inspection robot and evaluate the performance. The prototype is designed according to the following settings and the robot legs are made adjustable to be able to set angle θ at different values. The settings include: R=155mm, $W \leq$5kg,

Figure 8. The D-W_{load}-μ graph for a given R, W and θ

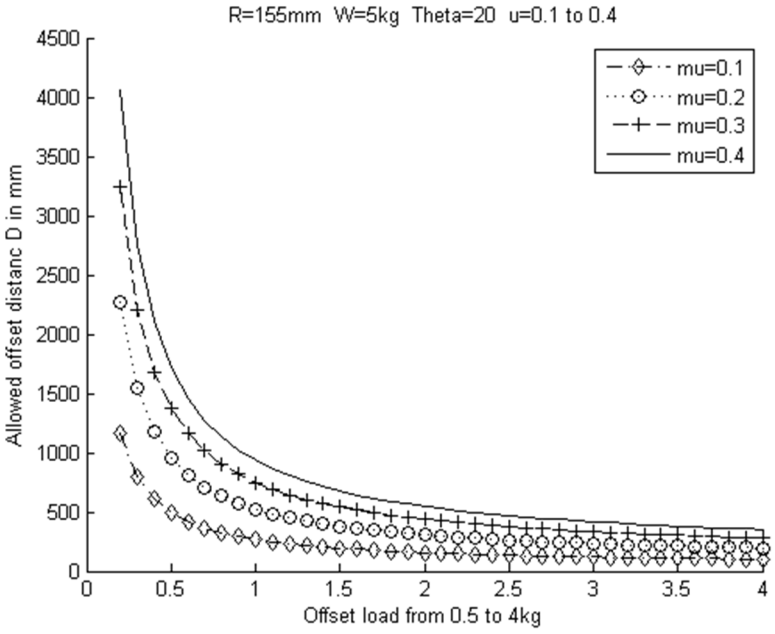

Figure 9. The D-R-μ graph for a given W, W_{load} and θ

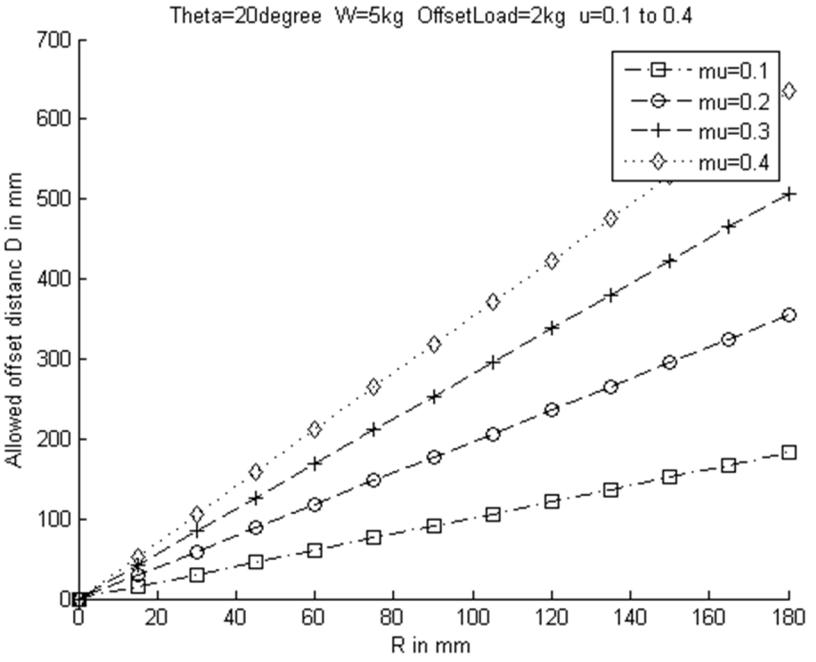

$W_{load} \leq 2$kg, and μ=0.1. Although the recommended sliding friction coefficient for tires on a concrete surface under wet muddy conditions is from 0.4 to 0.75 by Roymech.co.uk, to be conservative, the coefficient of friction μ=0.1 was used in the experiments to represent for the worst situation.

The main body of the test model is a rectangular aluminum platform, which is 400x300x10mm. The width of the platform reaches the maximum possible size within the specified pipe. The four robot legs join at the two ends of the platform using two half-circled brackets. Each bracket hosts two legs. Both brackets have a series of tapped holes on them, which allow the robot legs to be bolted on at different positions by rotating the robot leg around the joint. In such way, angel θ is adjustable. These holes are spaced at 10-degree intervals for the experiments. Smaller intervals or even multiple layers of circularly positioned holes can be used for fine θ angle adjustments. Once angle θ is selected, the robot legs are fixed on the bracket through a mechanical locker. Each leg has a roller wheel at the end. The design of the assembly allows angle θ changes from 10 to 80 degrees. From the above analysis it can be seen that angle θ will hardly take the extreme values although the large span means the robot has the potential to cope with wide applications. For the cases in this research, even for the severe pipe erosions, angle θ takes 20 degrees is small enough and provides plenty of space to cover the eroded bottom of the pipes including the cases where the bottom of the pipe might not exist as shown in Figure 1. It is not recommended for angle θ to take values greater than 45 degrees as higher values of θ may cause the robot to travel within the pipe unstably.

Two motors are used in the prototype development and both are geared motors. The output shaft of the motor has an offset from the centre, which makes it desirable for the test model as this gives more space for the actuation system to allow mounting of the wheel onto the output shaft. The design is also beneficial for using small wheels, which do not require further gearing down of the motor for the experiments. The wheel diameter used for the prototype is 20mm. This keeps the overall robot platform compact. The two wheels on the front legs are directly mounted onto the legs by using two small shafts, bushings and bearings.

Robot Platform Testing without Payload

In order to verify whether the robotic system is able to retain its starting orientation while it travels inside a pipe and evaluate the effect of angle θ, experiments without payload on the platform were first conducted. The assembled test system was placed within a pipe that had marks at the two ends of the pipe to identify any possible robot rolling when the pipe inspection robot travels from one end of the pipe to the other. The robot system was manually switched on and off using a 5A power supply.

The tests performed on the prototype demonstrated that the robotic platform was able to maintain its initial orientation for a wide range of angle θ. The tests also showed that, when angle θ was less than 20 degrees, the power required to drive the robot was significantly increased. This reveled that, as angle θ deceases, the normal forces caused by the robot gravity force applied on the wheels increase dramatically. The tests also found that, when angle θ was set at 20 degrees, the platform was able to firmly hold its starting orientation while it traveled through the pipe. This is important for the underground pipe inspection system of this research project to use real time vision system and accurately locate the eroded areas. If this had not been the case, a system would have been developed which could involve the use of either passive or active measures to self-stabilize the platform. This would have introduced a much greater level of complexity especially in the calibration of any inspection result around circular surface.

Robot Platform Testing with a Payload

Pipe inspection robots often have to carry sensing instruments, data recording devices

and communication units. Testing the robot platform with a payload is more close to the application reality. The payload was placed on the platform and offset from the centre line of the pipe. This made it possible to conduct the following two types of experiments.

- The maximum offset distance with a given payload
- The maximum payload with a given offset distance

Aluminum blocks were used as the test weights. The initial load was set at 0.5kg and then gradually increased up to 2.5kg. For the cases where angle θ takes 20 degrees, when the payload added up to 2.5 kg, the robot platform was still able to travel within the pipe without rolling. However, as the weight increased, the motor reached its limit and drew too much power. Figure 10 shows a test that purposely tilted the robot platform at the starting position with a 2.5kg load. The load was placed 80mm away from the centre line, which resulted in an approximately 2Nm torque. The offset distance was limited by the space inside of the pipe. The experiment showed the robot platform was able to keep its initial orientation when it traveled from one end of the pipe to the other end. Finally, the prototype was integrated with a vision system that weighed less than 2.5kg without offset except the gravity centre offset caused by the unsymmetrical part design of the vision system, which is minor if any. This means the robot with the vision system is under the condition that is much better than the test situation. It was deemed that the payload used in the test was much heavier than the vision system and the possible electronic devices to be implemented on the pipe inspection robot. The experimental results clearly showed that the robot body was able to keep its orientation and carry the vision system. From the experiments conducted on the robot platform, it is obvious that, for heavy loads, large motors must be considered, especially for the cases where angle θ needs to be set close to 20 degrees.

REAL TIME VISION FOR PIPE INSPECTION

Structured Lighting for Measuring Erosion Depth

Vision system and laser have been used for pipe inspection for different industrial applications (Kirkham et al., 2000; Duran et al., 2007; Guo et al., 2009). Structured lighting using triangulation between an active illumination source and a sensor (Shirai & Suva, 1971; West, 1983; Jarvis, 1983) is applied for measuring the depth of erosion. However, the curvature of the pipe complicates the process as structured lighting is generally used with a planar surface. To determine the effect of offsets, it is first necessary to determine where the laser stripe will appear within the image. Let the coordinates be defined as in Figure 11, with x along the direction of the pipe, y across the width of the pipe, and z vertically. Also, let the pipe radius be r, and the angles of the light stripe and camera be φ and θ, respectively. Further, it is assumed that the laser stripe along the bottom of the pipe (at the origin) is imaged to the centre of the field of view of the camera.

The intersection of the laser stripe forms an ellipse. If the position along this ellipse is parameterised by angle α, then coordinates of the points along the laser strip are:

$$\begin{aligned} y &= r\sin\alpha \\ z &= r(1-\cos\alpha) - d \\ x &= -z\tan\phi \end{aligned} \tag{11}$$

where d is the vertical depth of any erosion.

Transforming these points into camera centred coordinates provides the following.

$$\begin{aligned} x' &= y \\ y' &= \left(x - x_c\right)\cos\theta - \left(z - z_c\right)\sin\theta \\ z' &= -\left(x - x_c\right)\sin\theta - \left(z - z_c\right)\cos\theta \end{aligned} \tag{12}$$

Figure 10. Robot platform in experiments with a 2.5kg offset payload

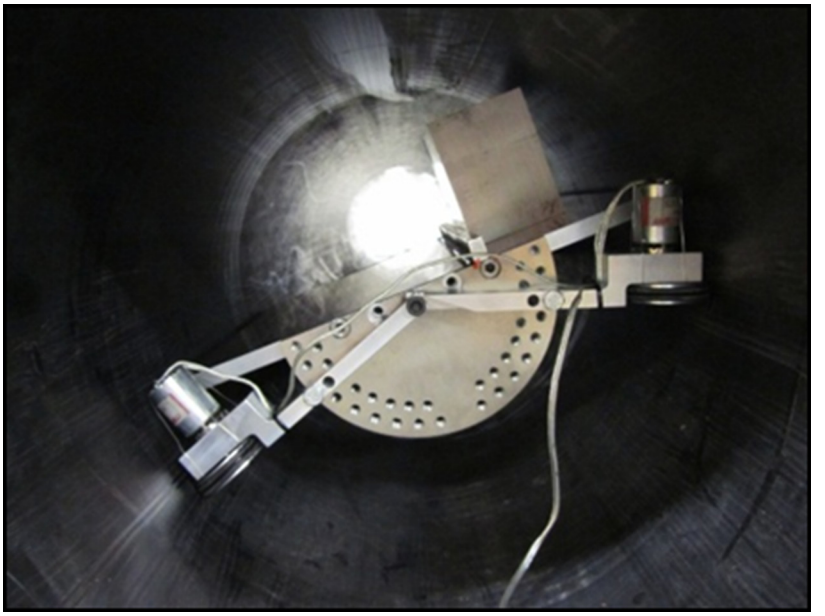

where the camera is located at $\left(\mathrm{x_c}, 0, \mathrm{z_c}\right)$. $(x_c, 0, z_c)$, and $x_c = z_c \tan\theta$

Therefore,

$$y' = (r\cos\alpha - r + d)\left(\tan\phi\cos\theta + \sin\theta\right)$$

$$z' = \left(r - r\cos\alpha - d\right)\left(\tan\phi\sin\theta - \cos\theta\right) + z_c / \cos\theta \quad (13)$$

Finally, a pinhole model of the camera is used to project the light stripe onto the sensor in image coordinates.

$$\hat{x} = f\frac{x'}{z'},\ \hat{y} = f\frac{y'}{z'} \quad (14)$$

Figure 11. The coordinate system and definition

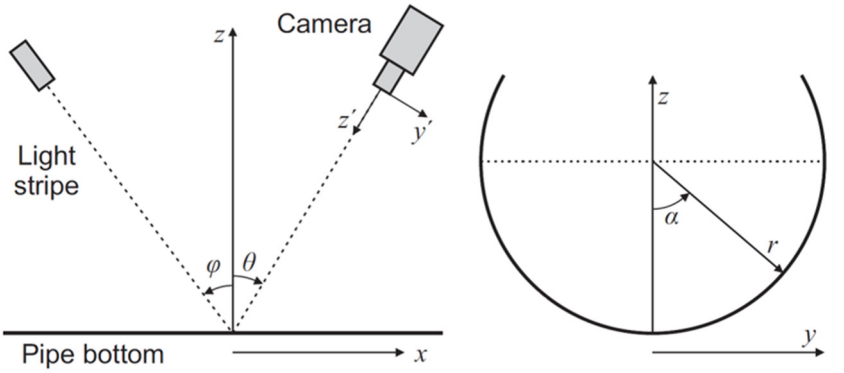

where f is the effective focal length of the lens (in pixels) and the origin for the image coordinates is defined to be in the centre of the image.

The lateral position within the pipe, y, is clearly mapped onto the horizontal position within the image captured. However, since the pipe surface is curved, the mapping is distorted by the scaling of the factor z'. The configuration used positions the laser vertically pointing down ($\phi = 0$) to the pipe. This configuration has the advantage that the laser stripe is on a fixed position along the length of the pipe (x = 0). Substituting $\phi = 0$ and (13) into (14) and eliminating α simplifies to

$$\hat{x} = f \frac{y cos\theta}{\left(\sqrt{r^2 - y^2} - r + d\right) cos^2\theta + z_c} \tag{15}$$

$$\hat{y} = f \frac{\left(\sqrt{r^2 - y^2} - r + d\right) sin\theta cos\theta}{\left(\sqrt{r^2 - y^2} - r + d\right) cos^2\theta + z_c} \tag{16}$$

There is a position dependent magnification of the image. Within the confines of the pipe, tilting the camera allows the distance from the camera to the bottom of the pipe to be lengthened, which reduces the overall magnification, and increases the field of view. The shift of the line within the image is approximately proportional to the depth of the erosion:

$$\Delta \hat{y} \approx \frac{df sin\theta cos\theta}{\left(\sqrt{r^2 - y^2} - r\right) cos^2\theta + z_c} \tag{17}$$

with the scale factor dependent on the lateral position within the image.

Image Processing

The image processing to detect the light stripe first determines the position of the light stripe in each column, then subtracts off the reference profile corresponding to no erosion. The result is then scaled and resampled to account for the varying magnification across the image.

With the red laser stripe, the maximum of the red component will generally give the position of the stripe. However, in situations where the reflectivity is low, the background may be brighter. The background may be removed effectively by subtracting the green component of the image from the red. This will have little effect on the laser stripe. Filtering the image with a 5x1 average filter smoothes the laser line and results in a better defined peak which can be detected more reliably.

The row number of the maximum pixel value in each column corresponds to the position of the laser line. Subtracting the reference level from the detected profile and then scaling the result using equation (17) to obtain the erosion depth. An example of the detected profile for an image captured with the angle of the camera $\theta = 40^\circ$, and with the reference profile overlaid is shown in Figure 12.

FPGA Implementation

The data processing in real time is far too much for using a low power embedded microcontroller. This may be overcome by processing the images in hardware using an FPGA. The images may be processed directly as they are streamed from the camera chip. This significantly reduces the memory requirements and improves the latency. The processing logic is shown in Figure 13.

Using a CMOS camera, the whole image does not need to be captured. By selecting and reading out only the region of interest, the frame rate may be increased. The data coming from the camera consists of raw pixel values as captured by the camera with the Bayer colour filter array (see Figure 14). Consequently, each individual pixel will only have one colour component. The blue pixels are not required, so only every second line of the input image needs to be processed. The adjacent green pixels can be averaged and subtracted from the centre red pixel. This can be implemented as a simple horizontal filter,

Figure 12. The detected profile

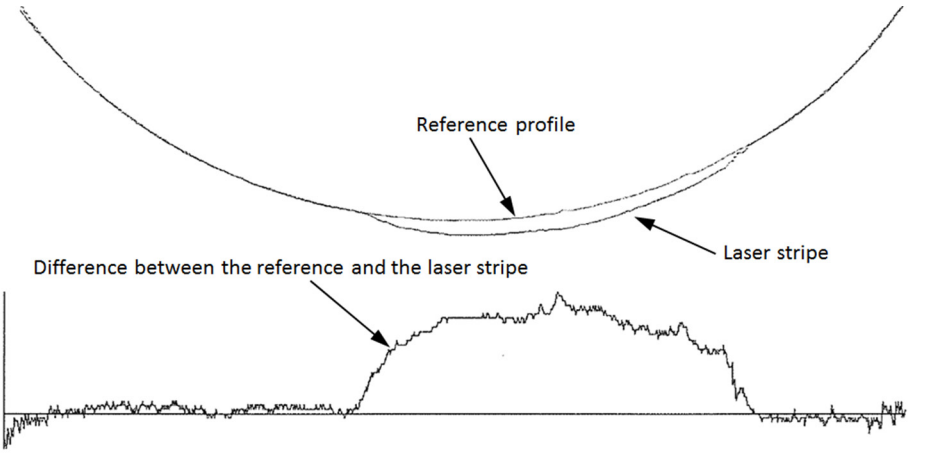

with the output register (and subsequent stages) clocked every second clock cycle.

The vertical smoothing filter processes all of the columns in parallel as the data is streamed in. A 5x1 window requires buffering the previous four rows of pixel values. Rather than average the pixels within the window, the pixels are simply summed. This removes the need to divide by 5.

Figure 13. Processing logic for measuring pipe erosion profiles

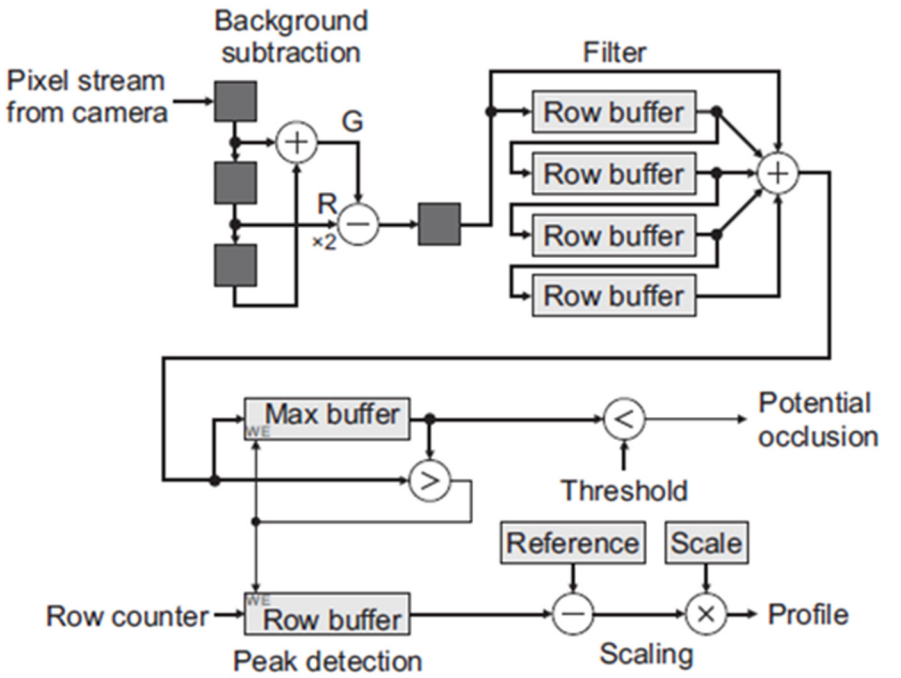

Figure 14. Bayer pattern with the red pixels highlighted

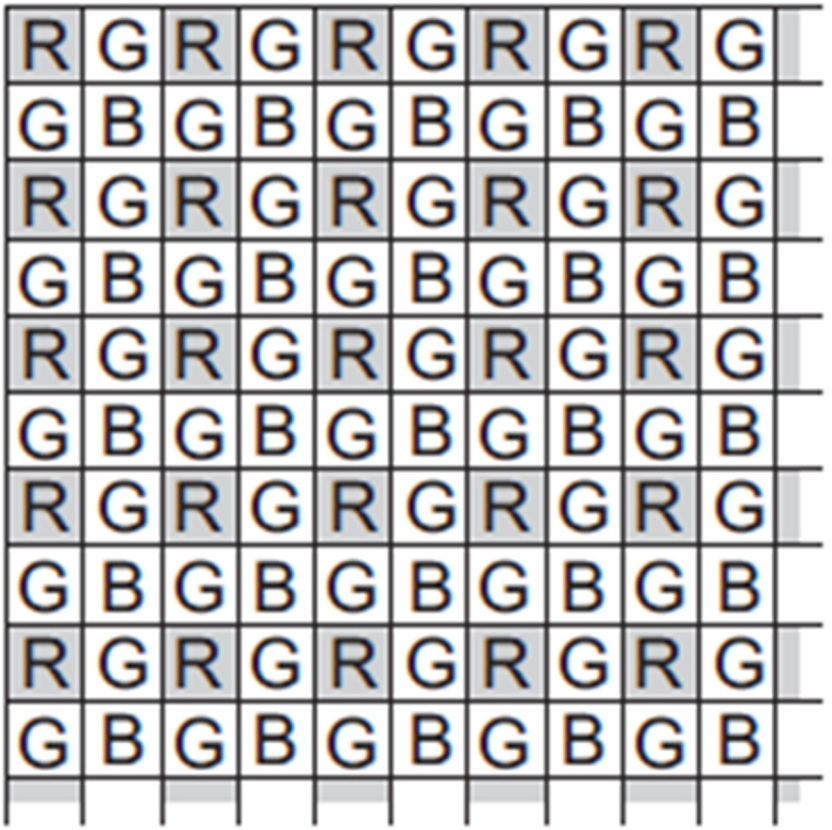

The current maximum value in each column is determined. It must be noted that the max buffer is cleared during the blanking period. Each pixel in the filtered pixel stream is compared with the corresponding column maximum at this time (read from the max buffer). If the new value is larger, then the value in the max buffer is replaced, and the corresponding row is recorded in the row buffer. At the end of the frame, the max buffer contains the maximum value in each column, and the row within the image that this occurred on is held in the row buffer.

The final stage, during the vertical blanking, is to convert the position of the laser stripe into an erosion profile. The laser stripe is read out from the row buffer, and the reference profile is subtracted from it. Finally, the difference is scaled to derive the depth in millimetres. The maximum value from the max buffer is compared with a predefined threshold and a flag is generated which indicates potential occlusions. At the same time that the maximum values are being acquired, the buffer is also cleared for the next frame.

The horizontal axis of the output erosion profile is distorted. If necessary, the output profile can be resampled to correct this. Such resampling can use a simple linear interpolation to generate the uniformly sampled profile. At this stage, resampling was not considered to be a requirement for the prototype system.

CONCLUSION AND FURTHER DEVELOPMENT

The research work and the experiments conducted prove the design concept of the rolling prevention mechanism is a feasible approach for underground pipe inspection robot. With the FPGA based vision system, it is possible to capture the cross-pipe profile, accurately locate the problem areas within a pipe, and process the image data in real time.

To build an entire map of the pipe erosion, determining the longitudinal position of the erosion and the corresponding cross-pipe erosion profile is essential. This can be achieved by implementing rotation based encoders on the robot wheels. As the robot travels down the pipe, the encoder can also trigger the capturing of the image and processing the data at regular intervals. The successive image capturing position data and the cross-pipe image profiles can then be used to build the entire pipe erosion map either in 2D or 3D model.

The FPGA based vision system processes the pixel data directly. As the data is streamed, the system significantly reduces the processing burden and effectively reduces the two dimensional image to a single line of data. The data rate is sufficiently reduced to be able to either stream the image data to flash memory (the DE0 board used supports directly writing to an SD card) (Terasic, 2009; Terasic, 2010) or to transmit the data wirelessly to an operator for immediate visualisation.

For wireless transmission, a ZigBee module could be connected via the DE0's RS232 port, with the profile data transferred at up to 17.7 frames per second without compression (with suitable data compression, this frame rate could easily be doubled.). Operating at this speed with a longitudinal resolution of 10 mm would take less than 6 seconds per metre of pipe inspected and measured. The image processing algorithm is currently being implemented on an FPGA platform, enabling a map of erosion within the pipe to be built at relatively high processing speeds while maintaining low operating power for battery operation.

REFERENCES

Budynas, R. G., & Nisbett, J. K. (2008). *Mechanical engineering design*. McGraw-Hill.

Duran, O., Althoefer, K., & Seneviratne, L. D. (2007). Automated pipe defect detection and categorization using camera/laser-based profiler and artificial neural network. *IEEE Transactions on Automation Science and Engineering*, *4*, 118–126. doi:10.1109/TASE.2006.873225

Guo, W., Soibelman, L., & Jr, J. H. G. (2009). Automated defect detection for sewer pipeline inspection and condition assessment. *Automation in Construction*, *18*, 587–596. doi:10.1016/j.autcon.2008.12.003

Jarvis, R. A. (1983). A perspective on range finding techniques for computer vision. *IEEE Transactions on Pattern Analysis and Machine Intelligence*, *5*, 122–139. doi:10.1109/TPAMI.1983.4767365 PMID:21869094

Kirkham, R., Kearney, P. D., Rogers, K. J., & Mashford, J. (2000). PIRAT – A system for quantitative sewer pipe assessment. *The International Journal of Robotics Research*, *19*, 1033–1053. doi:10.1177/02783640022067959

Norton, R. L. (2011). *Machine design*. Prentice Hall.

Pfeiffer, F., Robmann, T., & Loffer, K. (2000). Control of a tube crawling machine. In *Proc. Int. Conf. Control of Oscillations and Chaos* (vol. 3, pp. 586–591).

Roh, S. G., Ryew, S. M., Yang, J. H., & Choi, H. R. (2001), Actively steerable inpipe inspection robots for underground urban gas pipelines. In *Proc. IEEE Int. Conf. Robotics, Automation* (pp. 761–766).

Roman, H. T., Pellegrino, B. A., & Sigrist, W. R. (1993). Pipe crawling inspection robots: An overview. *IEEE Transactions on Energy Conversion*, *8*, 576–583. doi:10.1109/60.257076

Ryew, S. M., Baik, S. H., Ryu, S. W., Jung, K. M., Roh, S. G., & Choi, H. R. (2000). Inpipe inspection robot system with active steering mechanism. In *Proc. IEEE Int. Conf. Intelligent Robots, Systems* (pp. 1652–1657).

Shirai, Y., & Suva, M. (1971). Recognition of polyhedrons with a range finder. In *Proceedings of the International Joint Conference on Artificial Intelligence*, London, UK (pp. 80-87).

Terasic. (2009). *DE0 user manual* (vol. Version 1.4). Terasic Technologies.

Terasic. (2010). *TRDB-D5M 5 mega pixel digital camera development kit* (vol. Version 1.2). Terasic Techologies.

West, P. C. (1983). Machine vision in practice. *IEEE Transactions on Industry Applications*, *19*, 794–801. doi:10.1109/TIA.1983.4504290

Yaguchi, H., & Izumikawa, T. (2012). *Wireless in-piping actuator capable of high-speed locomotion by a new motion principle. IEEE Trans. Mech., 99*. Digital Object Identifier.

L. Tang received the BEng. degree in mechanical engineering from SWPU, China, 1982, and the PhD degree in mechanical engineering from the University of Liverpool, UK, in 1992. She was a research fellow with Gintic(SIMTech), Nanyang Technnlocal University, Singapore. Since 1996, she has been with Massey University, New Zealand, where she works in the School of Engineering and Advanced Technology. Her current research interests include mechatronics system design, robotics, intelligent control, biomechatronic engineering, and industrial automation.

D. Bailey received the B.E. (Hons) degree in Electrical Engineering in 1982, and the PhD degree in Electrical and Electronic Engineering from the University of Canterbury, New Zealand in 1985. From 1985 to 1987, he applied image analysis to the wool and paper industries within New Zealand. From 1987 to 1989 he was a Visiting Research Engineer at University of California at Santa Barbara. Dr Bailey joined Massey University in Palmerston North, New Zealand as Director of the Image Analysis Unit at the end of 1989. He is currently an Associate Professor in the School of Engineering and Advanced Technology, and leader of the Image and Signal Processing Research Group. His primary research interests include applications of image analysis, machine vision, and robot vision. One area of particular interest is the application of FPGAs to implementing image processing algorithms.

M. Jones received the BEng. degree in Mechatronics from Massey University, New Zealand in 2011. Since 2011, he has been with the School of Engineering and Advanced Technology, where he is currently working toward the MEng. degree in Mechatronics. His current research interests include mechatronics, robotics image processing, and FPGA.